methods

# DMS as an orthogonal separation to LC/ESI/MS/MS for quantifying isomeric cerebrosides in plasma and cerebrospinal fluid

**Hongbin Xu,[1,*,†] Frederic R. Boucher,[§] Thao T. Nguyen,[*,†] Graeme P. Taylor,[*,†] Julianna J. Tomlinson,[**,††] Roberto A. Ortega,[§§] Brigitte Simons,[§] Michael G. Schlossmacher,[**,††] Rachel Saunders-Pullman,[§§,***] Walt Shaw,[†††] and Steffany A. L. Bennett[1,*,†,**,††]**

Neural Regeneration Laboratory and India Taylor Lipidomics Research Platform,* Ottawa Institute of Systems Biology, Department of Biochemistry, Microbiology, and Immunology, University of Ottawa, Ottawa, Ontario, Canada; Centre for Catalysis Research and Innovation,[†] Department of Chemistry, University of Ottawa, Ottawa, Ontario, Canada; SCIEX,[§] Concord, Ontario, Canada; University of Ottawa Brain and Mind Research Institute,** Department of Cellular and Molecular Medicine, University of Ottawa, Ottawa, Ontario, Canada; Neuroscience Program,[††] Ottawa Hospital Research Institute, Ottawa, Ontario, Canada; Department of Neurology,[§§] Mount Sinai Beth Israel, New York, NY; Department of Neurology,*** Icahn School of Medicine at Mount Sinai, New York, NY; and Avanti Polar Lipids, Inc.,[†††] Alabaster, AL

**Abstract Cerebrosides, including glucosylceramides (GlcCers) and galactosylceramides (GalCers), are important membrane components of animal cells with deficiencies resulting in devastating lysosomal storage disorders. Their quantification is essential for disease diagnosis and a better understanding of disease mechanisms. The simultaneous quantification of GlcCer and GalCer isomers is, however, particularly challenging due to their virtually identical structures. To address this challenge, we developed a new LC/MS-based method using differential ion mobility spectrometry (DMS) capable of rapidly and reproducibly separating and quantifying isomeric cerebrosides in a single run. We show that this LC/ESI/DMS/MS/MS method exhibits robust quantitative performance within an analyte concentration range of 2.8–355 nM. We further report the simultaneous quantification of nine GlcCers (16:0, 18:0, 20:0, 22:0, 23:0, 24:1, 24:0, 25:0, and 26:0) and five GalCers (16:0, 22:0, 23:0, 24:1, and 24:0) molecular species in human plasma, as well as six GalCers (18:0, 22:0, 23:0, 24:1, 24:0 and 25:0) and two GlcCers (24:1 and 24:0) in human cerebrospinal fluid. Our method expands the potential of DMS technology in the field of glycosphingolipid analysis for both biomarker discovery and drug screening by enabling the unambiguous assignment and quantification of cerebroside lipid species in biological samples.**—Xu, H., F. R. Boucher, T. T. Nguyen, G. P. Taylor, J. J. Tomlinson, R. A. Ortega, B. Simons, M. G. Schlossmacher, R. Saunders-Pullman, W. Shaw, and S. A. L. Bennett. **DMS as an orthogonal separation to LC/ESI/MS/MS for quantifying isomeric cerebrosides in plasma and cerebrospinal fluid.** ***J. Lipid Res.*** **2019.** 60: **200–211.**

**Supplementary key words** lipidomics • liquid chromatography • mass spectrometry • tandem mass spectrometry • electrospray ionization • cerebrosides • sphingolipids • differential ion mobility spectrometry

Glycosphingolipids (GSLs) are essential plasma membrane lipid components of eukaryotes. Together with cholesterol and sphingomyelin, GSLs form microdomains on plasma membranes that play important roles in various cellular activities such as adhesion, growth, and differentiation (1). The simplest GSLs are monohexosylceramides (also known as cerebrosides). Cerebrosides are composed of a lipid, ceramide, that is embedded in the outer leaflet of the plasma membrane, and a sugar moiety, either glucose

*This work was supported by Canadian Institute of Health Research Grant MOP 311838 (S.A.L.B.), Natural Sciences and Engineering Research Council of Canada Grant RGPIN-2015-5377 (S.A.L.B.), National Institute of Neurological Disorders and Stroke Grant U01 NS094148 (R.S.P.), and the Weston Brain Institute (S.A.L.B., J.T., M.S., H.X.). The content is solely the responsibility of the authors and does not necessarily represent the official views of the National Institutes of Health.*

*Manuscript received 14 September 2018 and in revised form 31 October 2018.*

*Published, JLR Papers in Press, November 9, 2018*
*DOI https://doi.org/10.1194/jlr.D089797*

Abbreviations: CSF, cerebrospinal fluid; DMS, differential ion mobility spectrometry; CoV, compensation voltage; CV, coefficient of variation; DT, DMS temperature; GalCer, galactosylceramide; GalSph, galactosylsphingosine; GalT, UDP-galactose:ceramide galactosyltransferase; GCase, β-glucocerebrosidase; GlcCer, glucosylceramide; GlcSph, glucosylsphingosine; GlcT, UDP-glucose:ceramide β-1,1-glucosyltransferase; GSL, glycosphingolipid; HexCer, hexosylceramide; HexSph, hexosylsphingosine; HILIC, hydrophilic interaction chromatography; IPA, isopropanol; LLOD, lower limit of detection; LLOQ, lower limit of quantification; MRM, multiple reaction monitoring; NINDS, National Institute of Neurological Disorders and Stroke; PDBP, Parkinson's Disease Biomarkers Program; RP, reverse-phase; SCDase, sphingolipid ceramide *N*-deacylase; SV, separation voltage.

[1] To whom correspondence should be addressed.
e-mail: hxu@uottawa.ca (H.X.); sbennet@uottawa.ca (S.A.L.B.)

[S] The online version of this article (available at http://www.jlr.org) contains a supplement.

or galactose, that is attached to the ceramide by a β-glycosidic linkage. Galactosylceramide (GalCer) is the principal GSL in the brain and, together with its sulfated or sialylated derivatives, is an essential structural component of myelin. Glucosylceramide (GlcCer) is found in all mammalian membranes and is a major lipid component of skin and neurons. More complex GSLs can be further produced from GlcCer, to which additional sugar moieties and functional groups may be attached.

GlcCer and GalCer are synthesized by their respective synthases, the GlcCer synthase [UDP-glucose:ceramide β-1,1-glucosyltransferase (GlcT); EC 2.4.1.80] (2) and GalCer synthase [UDP-galactose:ceramide galactosyltransferase (GalT); EC 2.4.1.45] (3–6). The knockout and knockdown of these synthases have revealed critical biological relevancies (7–11). Both GlcCer and GalCer are essential to neural functions. GlcCer is involved in the axon growth of neural cells (12), and GalCer is indispensable for multiple myelin functions (8). Surprisingly, GalT-null mutants are still capable of myelination, albeit with reduced insulating capacity. While GalT knockout mice do not express any GalCers or their derivatives, they remain capable of synthesizing GlcCer using hydroxylated fatty acids, and they compensate for GalCer deficiency by incorporating GlcCer de novo into myelin (7, 8). By contrast, GalCer cannot compensate for neuronal GlcCer deficiencies. Brain-specific conditional knockout of GlcT is perinatal lethal with pups exhibiting structural and functional dysfunction in the cerebellum and peripheral nerves (11). Constitutive GlcT knockout is embryonic lethal, consistent with the essential role of GlcCer in the synthesis of complex GSLs throughout the body (9).

New methods that can quickly profile and reliably quantify cerebrosides are necessary for both diagnosing and understanding GSL disorders, as well as for drug screening. Cerebrosides are the natural substrates of β-glucocerebrosidase (GCase; EC 3.2.1.45) and β-galactocerebrosidase (EC 3.2.1.46). Humans with mutations in the *GBA* gene that encodes GCase, and thus with deficient degradation of GlcCer, may develop Gaucher disease. Those with deficient GalCer degradation develop Krabbe disease (13, 14). The molecular mechanisms underlying how GSL accumulation mediates these disorders are complex and not yet fully understood (15). For example, mutations in the human *GBA* gene that moderately decrease GCase activity significantly increase the risk of Parkinson's disease (16–18). Yet it is not clear how this impairment enhances Parkinson's disease risk. Elucidating the underlying mechanism is complicated by the technical challenges associated with discriminating between isomeric GlcCer and GalCer isoforms in biological samples. Both GlcCer and GalCer cerebrosides have virtually identical structures, with the only difference being the stereochemistry of the 4′-hydroxyl group as either axial (GalCer) or equatorial (GlcCer) (**Fig. 1**). GlcCer and GalCer isoforms also produce identical product ion spectra and possess similar physical properties, making their distinction very difficult by traditional LC/MS analysis.

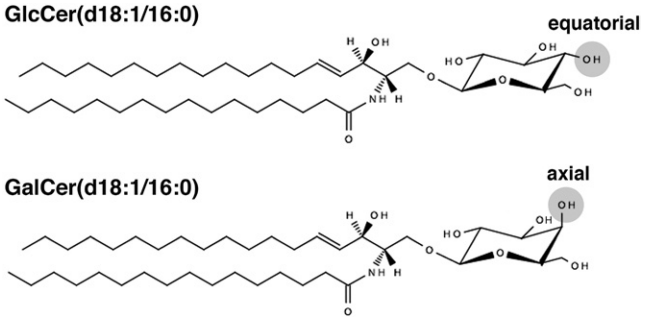


**Fig. 1.** Chemical structures of isomeric HexCers. Shown are structures of GlcCer(d18:1/16:0) and GalCer(d18:1/16:0). Both stereoisomers have the same Cer(d18:1/16:0) core structure to which a sugar molecule, glucose or galactose, is attached via β-glycosidic linkage. The only structural difference between these isomers is the 4′-hydroxyl group of the sugar moiety being either in the equatorial position (GlcCer) or axial position (GalCer).

To address this issue, we exploited recent advances in differential ion mobility spectrometry (DMS) to develop a simple, rapid, reliable method for profiling and quantifying GlcCer and GalCer isoforms in biological samples. DMS has emerged over the past decade as a viable addition to chromatography as an orthogonal separation technique that achieves highly selective multidimensional separations (19–21). This technique can be particularly useful in resolving isobaric and isomeric compounds in complex samples (22–25). As such, DMS has recently evolved as a powerful tool in the field of lipidomics (26, 27), yet its application in GSL analysis remains limited. Here, we explored the capabilities of DMS coupled with LC in ESI/MS/MS for differentially quantifying isomeric cerebrosides and their glucosylsphingosine (GlcSph) and galactosylsphingosine (GalSph) lyso forms. We show that 32 cerebroside species (16 isomeric GalCer-GlcCer pairs) and 1 pair of their GlcSph-GalSph metabolites can be separated in the DMS cell using isopropanol (IPA) as the gas-phase chemical modifier under the optimized conditions described here. Our results demonstrate robust quantitative performance, showing reproducibility and precision with a linear detection range of 2.8–355 nM. Using this method, we describe the profiling and quantification of GlcCer(d18:1/16:0), GalCer(d18:1/16:0), GlcCer(d18:1/22:0), GalCer(d18:1/22:0), GlcCer(d18:1/23:0), GalCer(d18:1/23:0), GlcCer(d18:1/24:1), GalCer(d18:1/24:1), GlcCer(d18:1/24:0), and GalCer(d18:1/24:0) as well as GlcCer(d18:1/18:0), GlcCer(d18:1/20:0), GlcCer(d18:1/25:0), and GlcCer(d18:1/26:0), but in the absence of their isomeric GalCer species in human plasma. We further detected and quantified GalCer(d18:1/18:0), GalCer(d18:1/22:0), GalCer(d18:1/23:0), GalCer(d18:1/24:0), GalCer(d18:1/24:1), and GalCer(d18:1/25:0) but only two GlcCer species [GlcCer(d18:1/24:0) and GlcCer(d18:1/24:1)] in human CSF. This study demonstrates the value of LC/ESI/DMS/MS/MS in the unambiguous assignment and reliable quantification of closely related stereoisomeric molecular species of cerebrosides and their lyso forms.

## MATERIALS AND METHODS

### Reagents

Methanol, chloroform, and IPA were purchased from Fisher Scientific Co. (Ottawa, Canada). Anhydrous ethanol was obtained from Commercial Alcohols (Brampton, Canada). Ammonium acetate, formic acid, HPLC-grade 1-propanol, and HPLC-grade 1-butanol were purchased from Sigma-Aldrich Canada Co. (Oakville, Canada). LC/MS-grade water and acetonitrile were purchased from Avantor Performance Materials (Central Valley, PA). Microwell plates were from Agilent Technologies Canada Inc. (Mississauga, Canada). Lipid standards, including GalSph(d18:1), GlcSph(d18:1), GalCer(d18:1/8:0), GlcCer(d18:1/8:0), GalCer(d18:1/16:0), GlcCer(d18:1/16:0), GalCer(d18:1/18:0), GlcCer(d18:1/18:0), GalCer(d18:1/24:1), and GlcCer(d18:1/24:1), were purchased from Avanti Polar Lipids, Inc. (Alabaster, AL). GlcCers and GalCers with 14:0, 16:1, 18:1, 20:0, 21:0, 22:0, 23:0, 24:0, 25:0, 26:0, 22:1, and 31:0 *N*-fatty acyl chains on the d18:1 sphingosine backbone were custom-synthesized by Avanti Polar Lipids, Inc. All lipid standards used in this study have a d18:1 sphingosine backbone with the sugar moieties attached via a β-glycosidic linkage.

### Human plasma and CSF sample preparation

Human blood from a 50-year-old Caucasian woman enrolled in the Ottawa Biobank Study was collected in $K_2$EDTA-coated lavender BD Hemogard tubes. The subject was assessed as cognitively normal using the Montreal Cognitive Assessment and Mini-Mental State Exam and had no significant acute medical illness (e.g., severely disturbed liver, kidney, or lung function), major psychiatric condition (e.g., major depressive disorder, schizophrenia, bipolar disorder), history of hospitalization for clinical stroke, or contraindication to MRI (e.g., metal in body, pacemaker). Consent was obtained in strict accordance with the Ottawa Hospital Research Institute Research Ethics Committee. The CSF sample was a pooled reference standard used to ensure normalization and standardization across sites, platforms, and assays and was from the National Institute of Neurological Disorders and Stroke (NINDS) Parkinson's Disease Biomarkers Program (PDBP). It was obtained in agreement with the National Institutes of Health and NINDS and the Icahn School of Medicine at Mount Sinai Research Ethics Committee as part of a study to evaluate pathway biomarkers for Parkinson's disease.

Each pair of isomeric GlcCers and GalCers was prepared by mixing the individual standard to a final concentration of 1 μM each in ethanol. Human plasma (100 μl) and human CSF (200 μl) were extracted using the modified method of Bligh and Dyer (28, 29), with an equimolar mixture of GalCer(d18:1/8:0) and GlcCer(d18:1/8:0) standards spiked in at the time of extraction for normalization. Extracted lipids were dried under a gentle stream of nitrogen gas at room temperature and were redissolved in ethanol. These lipid samples were stored in amber glass vials, flushed with nitrogen gas, and kept at −80°C until use.

### Infusion ESI/MS/MS analyses

Lipid samples were analyzed using a QTRAP 5500 triple quadrupole-linear ion trap mass spectrometer equipped with a Turbo V ion source (AB SCIEX, Concord, Canada). Source parameters (temperature, ionspray voltage, and gas flow) were optimized using a mixture of cerebroside standards that were T-infused with a syringe pump set at 5 μl/min into the flow of 10 μl/min of 100% solvent B (acetonitrile-IPA at a 5:2 v/v ratio containing 0.1% formic acid and 10 mM ammonium acetate) delivered by an Agilent Infinity II system (supplemental Table S1). A microfilter assembly (M-547; IDEX Health and Science, Oak Harbor, WA) was installed to prevent the potential blockage of the turbo-spray electrode (25 μm inner diameter) and contamination of the MS system. Nitrogen was used as curtain gas, collision gas, and ion source gas 1 and 2 unless otherwise stated. Compound parameters (declustering potential, entrance potential, collision energy, and collision cell exit potential) were individually optimized for each isomeric pair of cerebrosides and their lyso forms using the same method with the optimized source parameters. For these experiments, the DMS cell was physically installed but was set to "OFF" [DMS temperature (DT) set to "LOW" at 150°C by default)] during source and compound optimization.

### Infusion ESI/DMS/MS/MS method

DMS separation was performed in a SelexION differential ion mobility device interfaced with a triple quadrupole-linear ion trap mass spectrometer (QTRAP 5500; AB SCIEX). The DMS cell was mounted in the atmospheric pressure region between the curtain and the orifice plate of the mass spectrometer, and nitrogen was used as a transport gas. As compensation voltage (CoV) is influenced by mobile-phase and source conditions, DMS optimization was performed by injecting analytes at a flow rate and mobile-phase composition comparable to the intended LC conditions via T-infusion (see above). DMS parameters were optimized following the manufacturer's instructions using T-infusion of each isomeric pair of standards, and common parameters were determined as follows: DMS cell temperature = 150°C (low), modifier concentration = low (1.5% v/v in the transport gas, corresponding to a 173.8 μl/min flow rate for IPA), DMS resolution enhancement = 30 psi (medium) and DMS offset = −3.0 V, and nitrogen resolving gas = 30 psi. Four solvents, isopropanol, 1-propanol, 1-butanol, and methanol, were tested for their suitability as the DMS chemical modifier. To determine the optimal separation voltage (SV) and CoV pair for each isomeric pair of standards, CoV was ramped for each SV value in 100 V steps in the range of 3,000–4,100 V. Multiple reaction monitoring (MRM) spectra were recorded during CoV ramping, and the obtained data were plotted in the form of ionograms (signal intensity vs. CoV). With the highest signal intensity, a characteristic CoV value ensuring baseline or near-baseline separation was selected for each target analyte ion. CoV values at the peak apex were determined after Gaussian smoothing (smoothing width: 0.5 points for IPA and 1.5 points for 1-propanol, methanol, and 1-butanol). Lipid standards at 1 μM each in ethanol were used for DMS optimization.

### LC/ESI/DMS/MS/MS method

LC was performed with an Agilent Infinity II system operating at a flow rate of 10 μl/min with 8 μl (plasma) or 10 μl (CSF) sample injections by an autosampler maintained at 4°C. A 100 mm × 250 μm (inner diameter) capillary column packed with ReproSil-Pur 120 C8 (particle size of 3 μm and pore size of 120 Å) was used with a binary solvent gradient consisting of water with 0.1% formic acid and 10 mM ammonium acetate (solvent A) and acetonitrile-IPA (5:2; v/v) with 0.1% formic acid and 10 mM ammonium acetate (solvent B). The gradient started from 30% solvent B, reached 100% solvent B in 5 min, and was maintained for 30 min. The composition returned to 30% solvent B within 1 min and was maintained for 10 min to reequilibrate the column prior to the next sample injection. Data acquisition was performed in the positive ion mode using MRM with the optimized DMS parameters (see supplemental Table S2 for optimized DMS parameters and MRM transitions). Each duty cycle was 0.85 s, and the MRM data were acquired over the 45 min chromatography period.

Instrument control and data acquisition were performed with Analyst software version 1.6.2 (AB SCIEX). PeakView software

version 2.2.0 (AB SCIEX) was used for data processing and visualization. MultiQuant software version 3.0.2 (AB SCIEX) was used for processing quantitative MRM data.

## RESULTS

### Optimization of DMS separation

Source parameters were first optimized using a mixture of cerebroside standards that were T-infused with solvent B into the mass spectrometer (supplemental Table S1). Compound parameters were then optimized for each isomeric pair of GlcCer/GalCer and GlcSph/GalSph standards (supplemental Table S2). Collision energy was the only parameter that differed significantly between compounds, whereas declustering potential, entrance potential, and collision cell exit potential were all of very similar values (supplemental Tables S1, S2). For all standards, the precursor ion scan spectra showed the protonated $[M+H]^+$ ion as the base peak, and the product ion spectra showed the ion with $m/z$ 264.3 (corresponding to the didehydrated sphingosine) as the most intense fragment. Thus, the most intense MS/MS ion transition from $[M+H]^+ \rightarrow m/z$ 264.3 was monitored for each compound for DMS optimization and subsequent quantitative analyses.

With these optimized source and compound parameters, DMS was further optimized for the separation of isomeric GlcCer/GalCer and GlcSph/GalSph standards, with the intent of achieving the optimal separation with the best detection sensitivity. Experimental conditions were systematically varied by examining the influence of the main factors, including DT, transport gas type, SV, and the addition of gas-phase organic chemical modifiers, on DMS separation. DT influences DMS performance by affecting transport gas density and the clustering-declustering equilibrium of analytes according to the modifier (30, 31). We evaluated the three preset DTs on DMS performance mainly based on achieving the best sensitivity and found that the most intense and stable signals were obtained at the low setting of 150°C (supplemental Table S1). We next optimized SV and CoV simultaneously to find the SV and CoV combination that gave the best sensitivity and separation. The SV shifts the ion trajectories in the ion mobility cell, deviating ions from their central path entering the mass spectrometer. The CoV, a compound-specific parameter, compensates for the SV-causing shift of an ion trajectory, allowing specific ions to enter the mass spectrometer. We started with no chemical modifier added to the transport gas and noticed no separation of any of the isomeric analytes. It has been shown that the addition of gas-phase chemical modifiers drastically improves the separation power of the DMS (32–36). Indeed, the addition of polar organic chemical modifiers to the DMS cell resulted in partial or complete separation of isomeric compounds (**Fig. 2A**–D). Among the modifiers examined, IPA performed the best in terms of peak separation and sensitivity (Fig. 2D), followed by 1-propanol (Fig. 2C), 1-butanol (Fig. 2B), and methanol (Fig. 2A). However, with 1-butanol or methanol as modifiers, peaks were "noisier" and sometimes split. In addition, the isomeric hexosylceramide (HexCer) (d18:1/31:0) could not be effectively separated into GlcCer(d18:1/31:0) and GalCer(d18:1/31:0) isomers with methanol as a modifier. The effects of the modifier concentration were also investigated at the low and high settings. The use of a high concentration of modifiers resulted in an almost complete loss of signal. Thus, with IPA selected as a gas-phase chemical modifier at the low concentration setting, optimal SV and CoV values were determined for each pair of isomeric analytes by scanning the CoV over a range of fixed SVs (3,000–4,100 V at 100 V increments) using MRM in the positive ion mode.

Ramping the CoV during an MRM experiment resulted in the separation of isomeric species that can be visualized by their ionograms (Figs. 2, **3**). To verify the species identities corresponding to each CoV in the ionograms, lipid standards were injected individually while ramping the CoV. In all cases, the more negative CoV values corresponded to GlcCer and GlcSph species (Fig. 3). The optimized SVs ranged from 3,100 V for hexosylsphingosine (HexSph) to 4,000 V for HexCer(d18:1/31:0). Optimized SV and CoV values for all standards are listed in supplemental Table S2. These SV and CoV combinations resulted in baseline or near-baseline separation with the highest sensitivity. In general, the use of higher SVs shifted the ionograms to more negative CoVs and resulted in better separation but with decreased sensitivity (supplemental Fig. S1). The tradeoff between absolute signal intensity and improved signal-to-noise ratio was considered entirely acceptable when isomeric species were baseline or near-baseline separated while not drastically sacrificing limits of quantification. Although the highest SV value of 4,100 V can be used during compound-dependent DMS optimization with T-infusion, we subsequently noticed that arcing occasionally occurred at this SV setting during LC/ESI/DMS/MS/MS runs. A previous study has demonstrated that arcing can be suppressed by the addition of a small amount of a second modifier to the chemical modifier stream, which we have not implemented thus far (37). We also tested whether the use of different transport gases, nitrogen, or zero-grade air would affect the DMS performance. The use of zero-grade air as gas 1/gas 2 had no effects on peak separation, peak shape, and signal intensity (supplemental Fig. S2), but it did seem to prevent arcing in an extended period of runs. The optimized CoV values were constant for isomeric standards using either gas (nitrogen or zero-grade air) (supplemental Fig. S2). Data presented herein were acquired using IPA as the chemical modifier for DMS separation and nitrogen as gas 1/gas 2.

### LC/ESI/DMS/MS/MS method validation using lipid standards

With these optimized parameters for DMS separation, an LC/ESI/DMS/MS/MS method was developed for the quantitative analysis of isomeric HexCer and HexSph. Each MRM transition was assigned the characteristic SV and CoV values of the corresponding isomeric species (supplemental Table S2). In all cases, DMS sufficiently





JOURNAL OF LIPID RESEARCH ASBMB

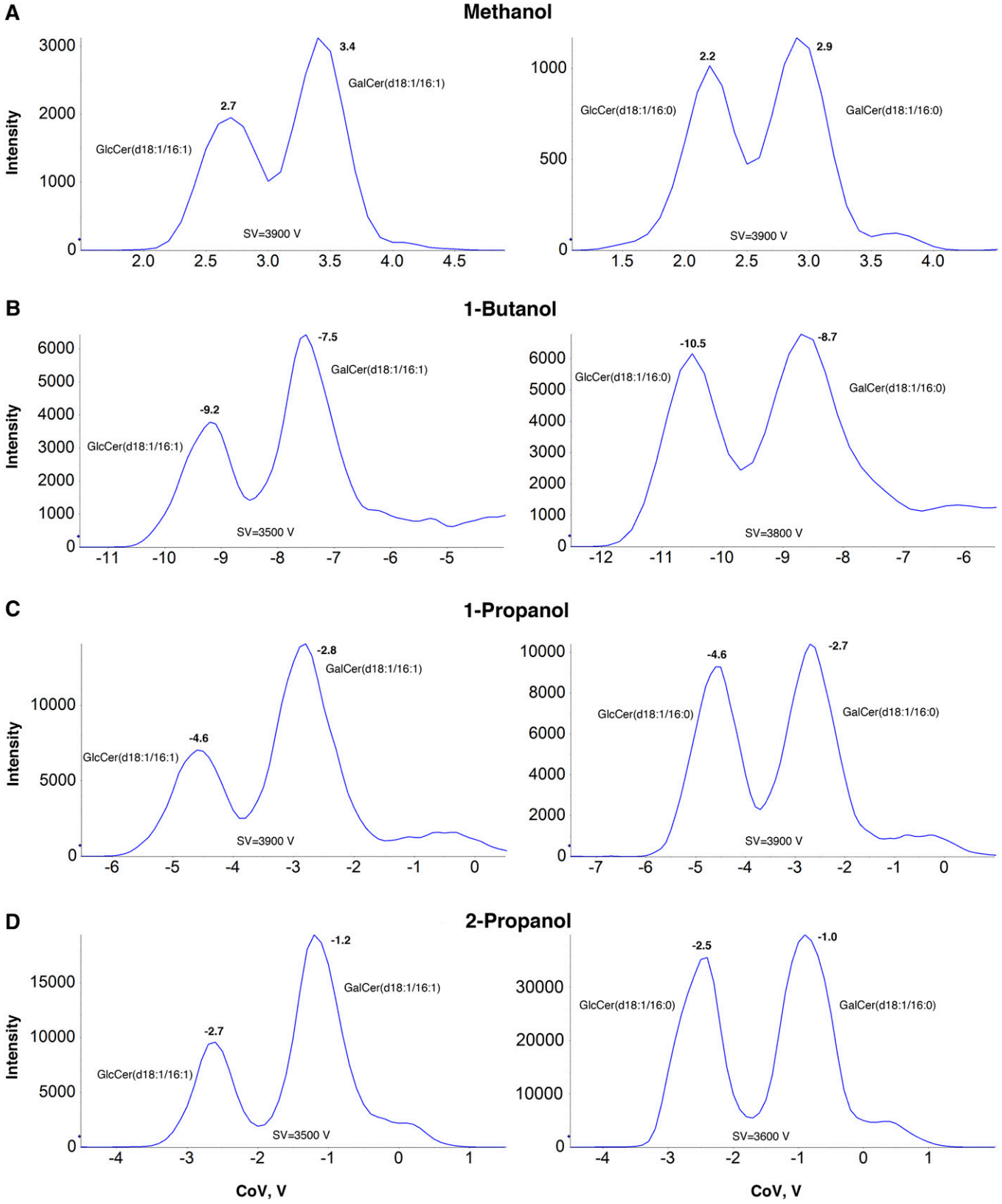


**Fig. 2.** Effects of adding gas-phase organic polar chemical modifiers on DMS separation. The addition of polar organic chemical modifiers, (A) methanol, (B) 1-butanol, (C) 1-propanol, or (D) 2-propanol, to the DMS cell resulted in partial or complete separation of isomeric compounds. Results for HexCer(d18:1/16:1) and HexCer(d18:1/16:0) are shown as representatives for species with unsaturated and saturated fatty acyl chains in the ceramide, respectively. The performance of the modifiers was assessed based on the resolution of peak separation and detection sensitivity. 2-Propanol provided near-baseline peak separation and the highest signal intensity, and its performance was followed by 1-propanol, 1-butanol, and methanol.

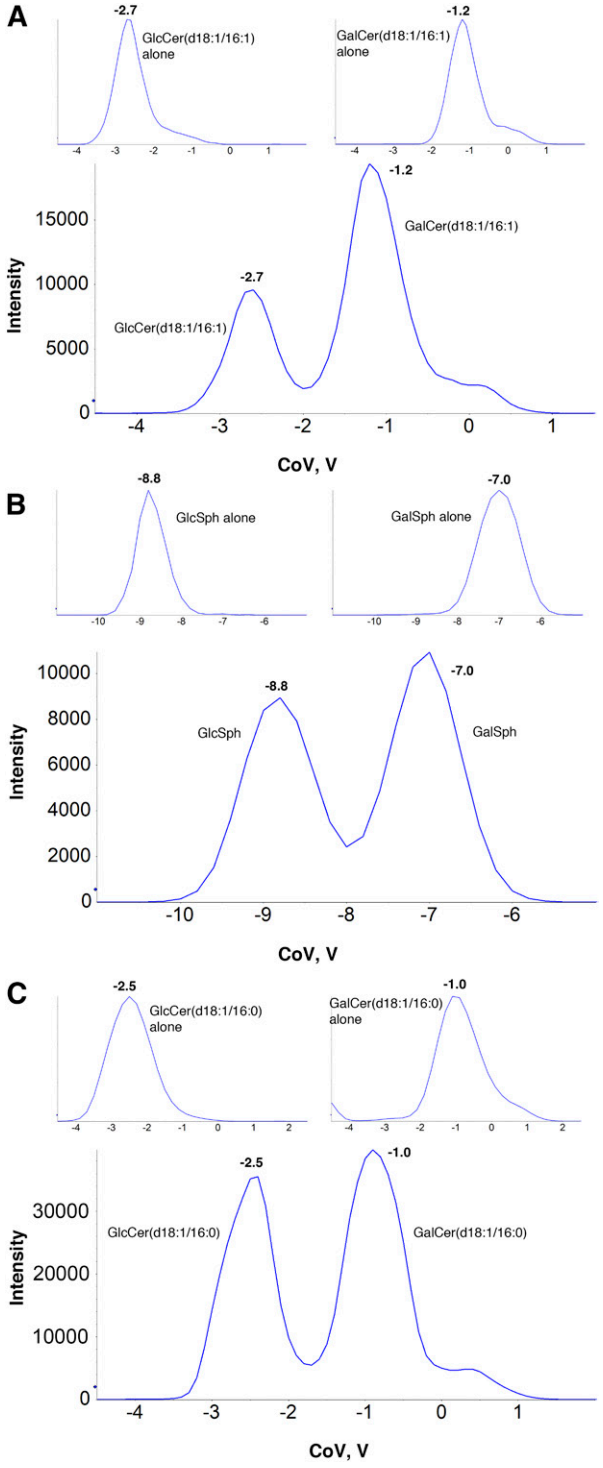


**Fig. 3.** Resolution of isomeric HexCer and HexSph species by DMS. GlcCer(d18:1/16:1) and GalCer(d18:1/16:1) (A), d18:1 GlcSph and d18:1 GalSph (B), or GlcCer(d18:1/16:0) and GalCer(d18:1/16:0) (C) were T-infused individually (insets in each panel) or as mixtures of isomeric pairs (main ionograms) and analyzed by DMS/MS in the positive ion mode using MRM. DMS effectively resolved isomeric species, enabling confirmation and independent quantification. In all cases, the more negative CoV values correspond to the glucosyl species. HexCer(d18:1/16:1) and HexCer(d18:1/16:0) are shown as representatives for species with unsaturated and saturated fatty acyl chains in the ceramide, respectively. HexSph is shown as the lyso form of HexCer.

separated isomeric species present in the mixture (**Fig. 4A–**C). As species with a different fatty acyl chain length and degree of unsaturation were separated by reverse-phase (RP) HPLC, coeluting isomeric species were isolated by DMS prior to entering the MS (Fig. 4B, C). Because DMS operates in the millisecond scale, there was little difference in retention time between isomeric species (Fig. 4B, C).

The linearity of the method was determined using a standard solution serially diluted nine times within a concentration range of 3–700 nM for all analytes except for HexCer(d18:1/8:0), which was spiked in at a constant amount in all runs to serve as an internal standard for normalization. Calibration curves were constructed using the ratio of the peak area of each GlcCer/GlcSph and GalCer/GalSph species to that of GlcCer(d18:1/8:0) and GalCer(d18:1/8:0), respectively. For HexSph and HexCer(d18:1/8:0), calibration curves were constructed with GlcCer(d18:1/18:0) and GalCer(d18:1/18:0) spiked in at a constant amount to each run of serially diluted standard mixtures containing HexCer(d18:1/8:0) and HexSph. **Table 1** summarizes the linear calibration parameters of all isomeric HexCer and HexSph standards. Standard curves obtained displayed good linearity with an average $R^2$ value of 0.987 (range: 0.961–0.998) within the tested dynamic range, demonstrating the capacity of this method in quantifying biologically relevant large changes in these glycosphingolipid levels. The sensitivity of the method was assessed by determining the lower limit of detection (LLOD) and lower limit of quantification (LLOQ) in triplicates, defined as the lowest analyte concentration with a signal-to-noise ratio of confirmatory precursor ions greater than 3 and 10, respectively. The LLOD and LLOQ values for all HexCer standards were estimated to be 0.9 and 3.0 nM or lower (not further assessed using more dilute samples), respectively (Table 1). These values were 5 and 10 times higher for GlcSph and GalSph compared with GlcCer and GalCer, respectively. The estimated LLOQ values were demonstrated to be sufficiently low for quantification in both 200 µl starting material of human CSF and 100 µl starting material of human plasma (see below).

The precision of this method was further assessed using a standard mixture containing an equimolar concentration (213 nM in the loading mixture) of all isomeric HexCer and HexSph species. The measured precision, indicated by the coefficient of variation (CV), ranged from 3.74% to 20.77%, with an average value of 10.70% for all standards (**Table 2**). These data demonstrate that DMS is capable of resolving a mixture of lipid standards with good quantitative precision. Given that the instrument response of each standard was different in LC/ESI/DMS/MS/MS (Fig. 4), these calculated ratios could be used as correction factors for subsequent quantification using GlcCer(d18:1/8:0) and GalCer(d18:1/8:0) as internal standards (Table 2).

### Quantitative analysis by LC/ESI/DMS/MS/MS of biological samples with a complex matrix

We next evaluated the capability of this method in resolving and quantifying HexCer and HexSph isomeric





JOURNAL OF LIPID RESEARCH

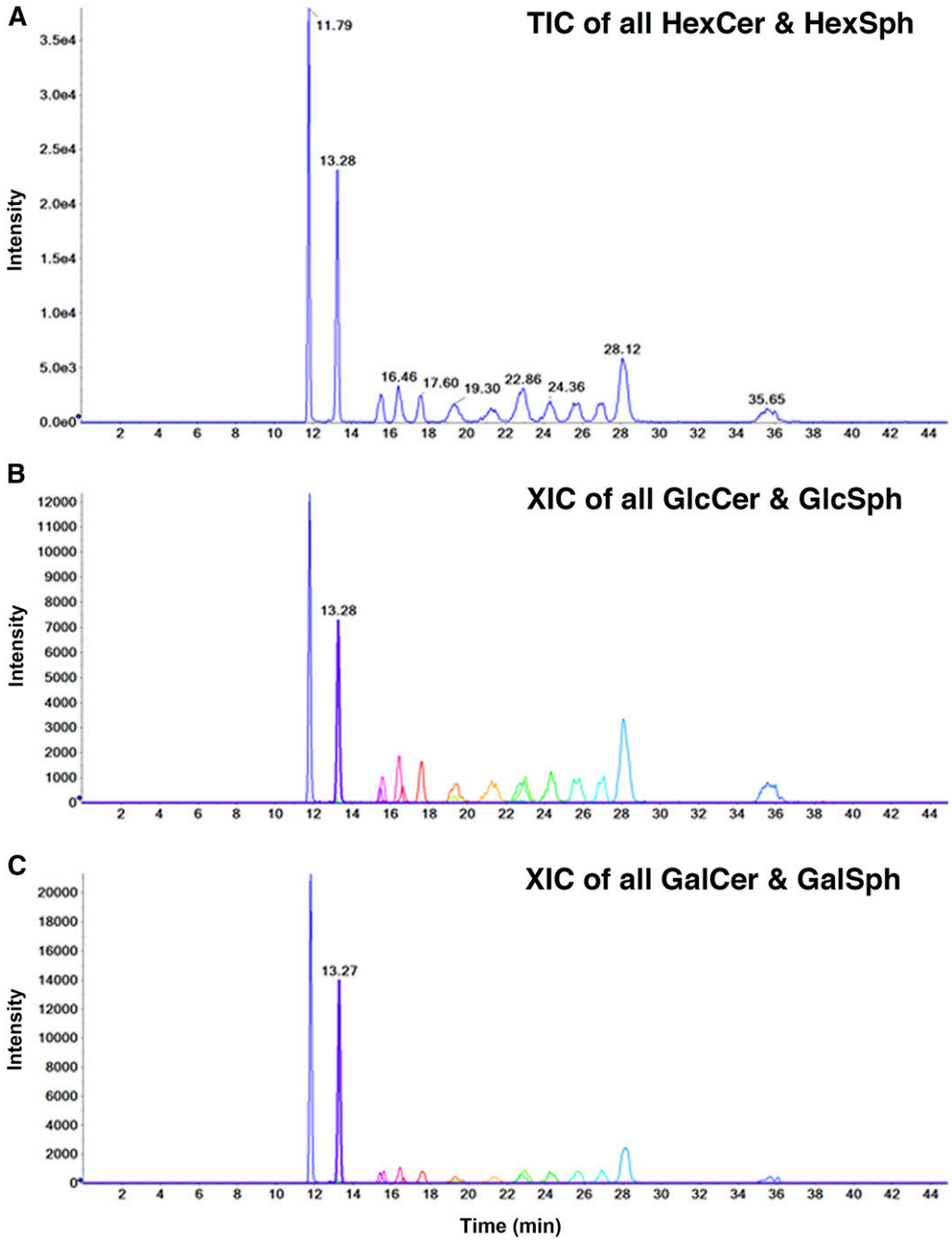


**Fig. 4.** Application of DMS with LC to enable the simultaneous quantification of isomeric HexCer and HexSph species. RP LC separation coupled with DMS allowed the complete resolution and independent quantification of every molecular species in the standard mixture (containing an equimolar concentration of all standards) by MRM. Each MRM transition was assigned the characteristic CoV value of the corresponding isomeric species. Shown are (A) TIC of all standards, (B) XIC of glucosyl species, and (C) XIC of galactosyl species. TIC, total ion chromatography; XIC, extracted ion chromatography.

species in biological samples with a complex matrix. Similar to the defined mixtures of lipid standards, DMS resolved the isomeric HexCer species present in human plasma and CSF effectively with excellent reproducibility in complex matrices (**Fig. 5**). To accurately quantify HexCer in biological samples, GlcCer(d18:1/8:0) and GalCer(d18:1/8:0) were spiked in at the time of lipid extraction as internal standards, enabling normalization to account for both extraction efficiency and instrument response differences. After normalizing the peak area of each detected species to that of the corresponding 8:0 species, correction factors (Table 2) were applied to calculate the amount of HexCer species. In human plasma, there was approximately eight times the amount of GlcCer compared with GalCer (10.92 ± 0.26 nmol/ml vs. 1.38 ± 0.15 nmol/ml) (Fig. 5D). Nine GlcCer species containing 16:0, 18:0, 20:0, 22:0, 23:0, 24:1, 24:0, 25:0, and 26:0 *N*-fatty acyl chains and five GalCer species containing 16:0, 22:0, 23:0, 24:1, and 24:0 *N*-fatty acyl

TABLE 1. Calibration curves, LLOD, and LLOQ of HexCer and HexSph standards

| FA[a] | GalCer | Calibration range (nM) | Slope | LLOD (nM) | LLOQ (nM) | GlcCcer | Calibration range (nM) | Slope | LLOD (nM) | LLOQ (nM) |
|---|---|---|---|---|---|---|---|---|---|---|
| 8:0 | 0.996 | 20–333 | 0.006 ± 0.000 | ND | ND | 0.985 | 20–333 | 0.002 ± 0.000 | ND | ND |
| 14:0 | 0.977 | 3–355 | 0.032 ± 0.002 | 0.9 | 3.0 | 0.991 | 3–355 | 0.033 ± 0.001 | 0.9 | 3.0 |
| 16:0 | 0.990 | 3–177 | 0.071 ± 0.003 | 0.9 | 3.0 | 0.990 | 3–177 | 0.169 ± 0.008 | 0.9 | 3.0 |
| 16:1 | 0.985 | 3–355 | 0.026 ± 0.001 | 0.9 | 3.0 | 0.993 | 3–355 | 0.045 ± 0.002 | 0.9 | 3.0 |
| 18:0 | 0.991 | 3–177 | 0.066 ± 0.003 | 0.9 | 3.0 | 0.990 | 3–355 | 0.159 ± 0.006 | 0.9 | 3.0 |
| 18:1 | 0.981 | 3–355 | 0.020 ± 0.001 | 0.9 | 3.0 | 0.983 | 3–355 | 0.061 ± 0.003 | 0.9 | 3.0 |
| 20:0 | 0.971 | 3–177 | 0.058 ± 0.005 | 0.9 | 3.0 | 0.978 | 3–355 | 0.146 ± 0.009 | 0.9 | 3.0 |
| 21:0 | 0.991 | 3–177 | 0.051 ± 0.002 | 0.9 | 3.0 | 0.992 | 3–355 | 0.127 ± 0.005 | 0.9 | 3.0 |
| 22:0 | 0.996 | 3–355 | 0.077 ± 0.002 | 0.9 | 3.0 | 0.997 | 3–355 | 0.155 ± 0.003 | 0.9 | 3.0 |
| 22:1 | 0.961 | 3–177 | 0.061 ± 0.005 | 0.9 | 3.0 | 0.971 | 3–355 | 0.086 ± 0.006 | 0.9 | 3.0 |
| 23:0 | 0.976 | 3–355 | 0.076 ± 0.005 | 0.9 | 3.0 | 0.992 | 3–355 | 0.191 ± 0.007 | 0.9 | 3.0 |
| 24:0 | 0.981 | 3–355 | 0.086 ± 0.005 | 0.9 | 3.0 | 0.993 | 3–355 | 0.188 ± 0.006 | 0.9 | 3.0 |
| 24:1 | 0.991 | 3–177 | 0.053 ± 0.002 | 0.9 | 3.0 | 0.996 | 3–355 | 0.164 ± 0.004 | 0.9 | 3.0 |
| 25:0 | 0.980 | 3–355 | 0.068 ± 0.004 | 0.9 | 3.0 | 0.993 | 3–355 | 0.157 ± 0.005 | 0.9 | 3.0 |
| 26:0 | 0.983 | 3–355 | 0.231 ± 0.012 | 0.9 | 3.0 | 0.992 | 3–355 | 0.459 ± 0.017 | 0.9 | 3.0 |
| 31:0 | 0.995 | 3–177 | 0.058 ± 0.002 | 0.9 | 3.0 | 0.998 | 3–355 | 0.147 ± 0.003 | 0.9 | 3.0 |
| 0:0 | 0.994 | 16–532 | 0.002 ± 0.000 | 10.0 | 33.2 | 0.993 | 16–532 | 0.001 ± 0.000 | 5.0 | 16.6 |

The concentration is of lipid standards in the MS loading mixture. ND, not determined.
[a]Carbon number and degree of unsaturation of *N*-acyl chain in the ceramide moiety (e.g., 16:0 for fatty acyl chain with 16 carbons and zero double bonds).

chains were detected and quantified in the plasma (Fig. 5E). The most abundant species was GlcCer(d18:1/24:0) at 4186.00 ± 118.10 pmol/ml, whereas GlcCer(d18:1/26:0) at 15.42 ± 2.10 pmol/ml was the least abundant (Fig. 5E). The precision of quantifying the method with human plasma, as indicated by CV, was similar to that of pure standards (supplemental Table S3). In human CSF, six GalCer species (18:0, 22:0, 23:0, 24:0, 24:1, and 25:0) and two GlcCer species (24:0 and 24:1) were detected and quantified, with GalCer(d18:1/24:1) being the most abundant at 242.80 ± 19.72 pmol/ml and GlcCer(d18:1/24:0) being the least abundant at 8.25 ± 0.83 pmol/ml (Fig. 5F).

## DISCUSSION

We report here a new LC/ESI/MS/MS methodology that exploits DMS as an orthogonal separation to LC capable of rapidly, reproducibly, and efficiently separating and quantifying HexCer isomers into their constituent GalCer and GlcCer pairs in complex biological matrices. One of the biggest challenges in the field of lipidomics is quantifying isobaric lipid species both within and between lipid classes. In this regard, as well as in considering ion suppression in shotgun analysis, LC/ESI/MS/MS has become the method of choice in the analysis of complex biological samples. However, no single LC method is capable of effectively resolving all lipid species due largely to their diverse structures and biophysical properties. This necessitates alternative approaches such as the one used herein in which the orthogonal separation of complex samples following LC and prior to MS analysis enables simultaneously differentiating and quantifying HexCer isomers and HexSph isomers.

Isobaric GlcCer/GlcSph and GalCer/GalSph species share virtually identical chemical structures, making resolution by conventional LC/MS analysis very difficult. The most commonly used method does not exploit the quantitative sensitivity of LC/MS but instead utilizes a borate-coated TLC plate to separate GlcCer from GalCer (38). While effective in separation, this method suffers from low sensitivity and reproducibility. Normal-phase HPLC methods with (39, 40) or without derivatization (41, 42) have been developed for differentiating isomeric GlcCer and

TABLE 2. Precision of the method using lipid standards and CFs for quantification

| | FA[a] | | | | | | | | | | | | | | | |
|---|---|---|---|---|---|---|---|---|---|---|---|---|---|---|---|---|
| | 0:0 | 14:0 | 16:0 | 18:0 | 20:0 | 21:0 | 22:0 | 23:0 | 24:0 | 25:0 | 26:0 | 31:0 | 16:1 | 18:1 | 22:1 | 24:1 |
| GlcSph and GlcCer | | | | | | | | | | | | | | | | |
| Mean | 1.598 | 0.093 | 0.383 | 0.405 | 0.440 | 0.536 | 0.474 | 0.550 | 0.493 | 0.423 | 1.430 | 0.582 | 0.185 | 0.119 | 0.151 | 0.482 |
| SEM | 0.154 | 0.004 | 0.008 | 0.010 | 0.033 | 0.033 | 0.042 | 0.042 | 0.017 | 0.024 | 0.060 | 0.019 | 0.012 | 0.010 | 0.011 | 0.022 |
| CV (%) | 16.63 | 8.72 | 4.08 | 4.68 | 15.08 | 12.47 | 17.64 | 15.12 | 6.87 | 11.33 | 8.32 | 6.44 | 13.07 | 14.41 | 14.38 | 8.91 |
| CF | 1.598 | 0.093 | 0.383 | 0.405 | 0.440 | 0.536 | 0.474 | 0.550 | 0.493 | 0.423 | 1.430 | 0.582 | 0.185 | 0.119 | 0.151 | 0.482 |
| GalSph and GalCer | | | | | | | | | | | | | | | | |
| Mean | 1.443 | 0.092 | 0.134 | 0.123 | 0.121 | 0.151 | 0.215 | 0.195 | 0.229 | 0.189 | 0.572 | 0.160 | 0.084 | 0.050 | 0.064 | 0.128 |
| SEM | 0.119 | 0.003 | 0.009 | 0.008 | 0.005 | 0.011 | 0.005 | 0.005 | 0.013 | 0.007 | 0.023 | 0.004 | 0.009 | 0.005 | 0.001 | 0.008 |
| CV (%) | 14.24 | 7.13 | 12.74 | 13.28 | 8.38 | 13.88 | 4.81 | 4.98 | 11.58 | 7.60 | 7.96 | 5.15 | 20.77 | 16.28 | 3.74 | 11.90 |
| CF | 1.443 | 0.092 | 0.134 | 0.123 | 0.121 | 0.151 | 0.215 | 0.195 | 0.229 | 0.189 | 0.572 | 0.160 | 0.084 | 0.050 | 0.064 | 0.128 |

The mean values are the ratios of GlcCer and GalCer species to GlcCer(d18:1/8:0) and GalCer(d18:1/8:0), respectively, from quadruplicate experiments. CF, correction factor.
[a]Carbon number and degree of unsaturation of *N*-fatty acyl chain in the ceramide moiety (e.g., 16:0 for fatty acyl chain with 16 carbons and zero double bonds).

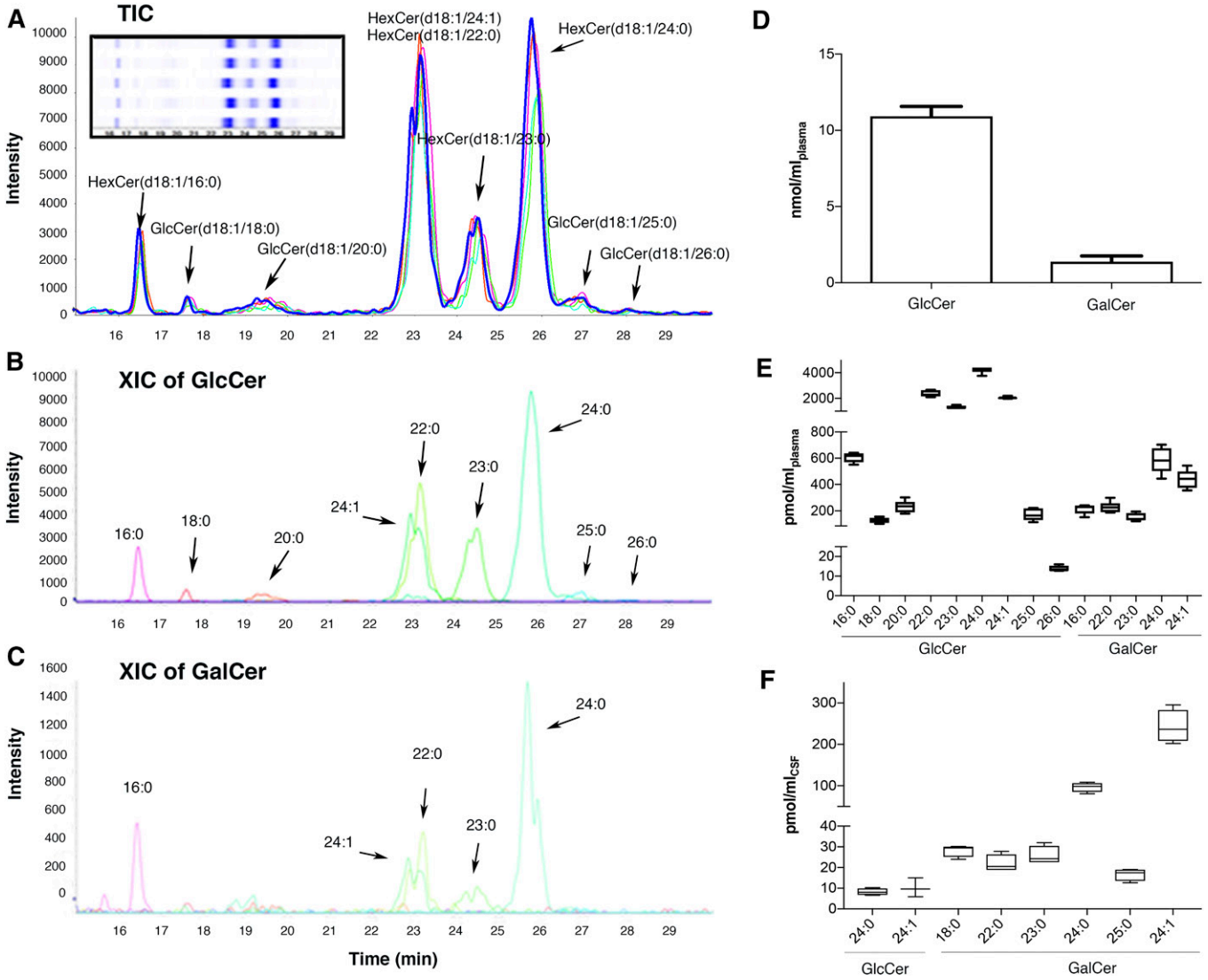


**Fig. 5.** LC/DMS/MS/MS allows the unambiguous assignment and simultaneous quantification of HexCer and HexSph species in human plasma and CSF. RP LC separation coupled with DMS allowed the specific quantification of GlcCer and GalCer isomeric species in human plasma and CSF. A: TIC overlay of LC/DMS/MS/MS runs ($n = 5$) of human plasma lipid extract showing chromatographic separation of HexCer species based on *N*-acyl chain composition with good reproducibility. Heat map representations of the chromatograms are shown in the inset. XIC of the nine GlcCer and five GalCer species in human plasma are shown in panels B and C, respectively. D: Total amounts of GlcCer and GalCer in human plasma are expressed as nmol/ml plasma. Data are expressed as mean ± SEM. Amounts of GlcCer and GalCer species in (E) human plasma and (F) CSF ($n = 4$) are expressed as pmol/ml plasma and pmol/ml CSF, respectively. Data are plotted in a box-and-whiskers format showing the median (line) and 25th to 75th percentiles (box), with whiskers extending to the minimum and maximum values. *n*, number of technical replicates of a single plasma or CSF lipid extract, respectively; TIC, total ion chromatography; XIC, extracted ion chromatography.

GalCer. For example, Kaye and Ullman (39) developed a method that required the synthesis of perbenzoylated derivatives of GlcCer and GalCer. However, isolating cerebrosides by silica gel chromatography before their derivatization is laborious and time-consuming. The added isolation and derivatization steps may also introduce additional quantitative errors. A more sensitive normal-phase HPLC-based method was later developed by analyzing *O*-phthalaldehyde derivatives of GlcSph and GalSph that are generated after treatment with sphingolipid ceramide *N*-deacylase (SCDase) (40). SCDase hydrolyzes the *N*-acyl linkage of the ceramide moiety of various GSLs, generating lyso forms of GSLs and releasing fatty acids (43). However, this enzyme also hydrolyzes sphingomyelin and possibly, to a lesser extent, ceramides, which is undesirable if the samples are to be concomitantly analyzed for these lipid subclasses. Furthermore, if HexSphs are present, this method would, by necessity, lead to an overestimation of HexCer. Conversely, if HexSphs are also of research interest, the same sample would need to be derivatized twice with or without SCDase treatment for the quantification of HexCer plus HexSph or HexSph, respectively. Recent methodological improvements in normal-phase HPLC have enabled direct and specific measurement of HexCer isomers without derivatization (41, 42). Although normal-phase HPLC allows for near-baseline separation of GlcCer and GalCer, molecular species within each family are still not completely resolved (42). This is not surprising given that normal-phase

LC separates analytes based on structural differences within the hydrophilic regions (i.e., galactose vs. glucose in this case), which interact with the normal phase. This may lead to the masking of low-abundant species by highly abundant ones due to ion suppression. Another potential issue is the interference caused by compounds with overlapping precursor-product ion pairs. For example, the M+2 isotopic component of HexCer(d18:1/24:1) will interfere with the quantification of HexCer(d18:1/24:0), especially when the former exists at much higher abundance. More recently, the hydrophilic interaction chromatography (HILIC) method has gained popularity in GlcCer and GalCer separation (44–46). Particularly worth noting is the development of a novel HILIC method using a more hydrophobic starting solvent to allow not only baseline resolution of GlcCer and GalCer with great detection sensitivity [LLODs of 2 and 7 ng/ml for GlcCer and GalCer, respectively, which is similar to the LLODs of 3 nM or 2.4 ng/ml for HexCer(d18:1/24:1) reported using our method] but also separation of α- and β-anomers (46). The added capability of this improved version of the HILIC method may be important because gut microbiota have been shown to produce α-GalCer that may appear in plasma under pathological conditions (46, 47) and thus should be differentiated from the normal β-anomers. Moreover, α-anomers have been shown to be made by mammalian immune cells in small quantities, necessary for natural killer T-cell homeostasis (48). These α-anomers, therefore, also contain the same mammalian ceramide anchors and are isobars. Similar to normal-phase LC, HILIC exploits differences within the hydrophilic regions of analytes to achieve separation. Even with improved resolution, it does not completely resolve molecular species of GlcCer or GalCer with a similar lipid anchor. Thus, it will be critical to establish whether DMS can be used to expand these analyses. Considering the complexity of lipidomes from cells, tissue, and bodily fluids, an ideal quantitative lipidomic workflow would consider the coupling of normal-phase LC with RP LC prior to MS analysis. Normal-phase LC separates lipid classes by their polar head groups (hydrophilicity), whereas RP LC separates lipid molecular species within each class based on their hydrocarbon chain composition (hydrophobicity). Combining the two exploits the amphiphilic properties of lipids and ensures the best resolution with minimal interference in MS detection. Successful online coupling of the two LC methods, however, has yet to be reported in practice.

Together, these challenges highlighted to us the potential of optimizing an RP HPLC/ESI/DMS/MS/MS methodology for HexCer and HexSph separation and quantification. The advent of DMS technology, especially when coupled with LC/ESI/MS/MS, has proven to resolve compounds that are indistinguishable by MS alone or by LC/MS (25, 26, 33). Ions are separated by their differential motility due to differences in size, shape, and interactions with gas-phase polar organic chemical modifiers, thereby providing high selectivity with minimal background interference (31, 33, 49). Here, we investigated the application of DMS technology coupled with RP HPLC to determine its utility as an orthogonal separation to LC for isolating isomeric HexCer and HexSph species. Our results demonstrate that isomeric HexCer and HexSph species were sufficiently separated in the DMS cell with IPA as a gas-phase chemical modifier under the optimized conditions. This method exhibited excellent quantitative performance, with reproducibility and precision within a linear detection range of 2.8–355 nM. In terms of detection sensitivity, despite an observed ∼20–40-fold drop of overall signal intensity when DMS is used compared with LC/MS alone without DMS, the estimated LLOQ and LLOD were within 10-fold differences. This was primarily due to the much reduced background noise levels with the use of DMS, consistent with previous observations (31, 33, 49).

Lipidomic analyses using this method have revealed the presence of both GlcCer and GalCer isomers defined by a d18:1 sphingosine backbone and 16:0, 22:0, 23:0, 24:0, and 24:1 fatty acyl chains as well as GlcCers with 18:0, 20:0, 25:0, and 26:0 fatty acyl chains in healthy human plasma with reproducible quantification over successive analyses (Fig. 5). In general, our data corroborated previous results well, showing that human plasma contained both GlcCer and GalCer (50, 51), with higher proportions of GlcCer. Quantitatively, we obtained 12.3 nmol/ml total cerebroside in human plasma compared with 9.4 and 9.8 nmol/ml reported by Wells and Jones (50) and Vance and Sweeley (51), respectively, and with C22:0, C23:0, and C24:0 as the major *N*-fatty acyl chains. We also noticed some discrepancies between our data and those published by Quehenberger et al. (52). A number of factors may have contributed to the discrepancies, including the source of plasma (e.g., pooled plasma from healthy people representing the ethnic distribution of the US population vs. single individual plasma used in this study), lipid extraction protocol, LC/MS protocol (e.g., two-step LC/MS protocol composed of initial quantification of cerebroside molecular species without differentiating isomeric GalCer and GlcCer, followed by a determination of the percentage composition of each isomer in a separate experiment vs. our one-step LC/MS protocol), and choice of standards. By using this method, we have also detected and quantified six GalCer (18:0, 22:0, 23:0, 24:0, 24:1, and 25:0) and two GlcCer (24:0 and 24:1) species in human CSF (Fig. 5f). Little information is available in the literature about cerebroside levels in human CSF. Indeed, this study represents one of the first methodologies capable of quantifying GalCer and GlcCer isomers from small volumes of CSF. A recent study by Seyer et al. (53) using high-resolution MS revealed the presence of five HexCer species in human CSF with semiquantitative information. Four of the five species reported were also detected and quantified in our study, except for HexCer(d18:2/24:1), for which we lack synthetic standards. However, due to the identical atomic composition of isomeric HexCer species, high-resolution MS is unable to resolve them.

To our knowledge, this is the first report to combine DMS technology with LC/ESI/MS/MS for the complete profiling of cerebrosides and their lyso forms in biological samples, notably CSF. We report here the DMS optimization of CoV values for each analyte [e.g., isomeric





JOURNAL OF LIPID RESEARCH ASBMB

GlcCer(d18:1/16:0) and GalCer(d18:1/16:0)]. Thus, pure standards must be available for each compound of interest. This is especially true when the isobaric species produce identical product ions, as seen here for isomeric GlcCer and GalCer. Thus, our capacity to differentiate these isobaric species is limited by the number of standards available. The strict requirement for standards is advantageous in that each compound is quantified using optimized compound-specific parameters. However, it also represents the biggest limitation of this method. In this context, even though we have routinely identified hydroxy fatty acid and phytosphingosine containing HexCer in a mammalian source, due to the lack of available standards we are unable to characterize their sugar moieties by DMS. Alternatively, if we can find and determine the relationship of a series of closely related compounds to their optimal CoV characteristics, we will be able to greatly increase our capacity to use DMS to analyze a family of compounds without the need of having pure standards for each and every analyte. In this study, we focused on achieving baseline or near-baseline separation without significantly sacrificing sensitivity given the decrease of signal intensity with increasing SV values. As such, both SV and CoV were optimized for each isomeric HexCer and HexSph. Future studies will aim to find relationships between analytes and their characteristic CoV values while keeping a constant SV so that, with only a few standards, an entire family of closely related compounds can be analyzed. Despite the limitation in the requirement of compound-specific standards, their usage represents the most accurate quantification strategy. The proper selection and use of internal standards are instrumental to quantitative lipidomics by MS. Conventionally, one (or a few) nonnaturally occurring standards with similar structures to the analytes of interest is used with the assumption that the standards and analytes all have the same instrument responses. However, this is rarely the case due to differences in ionization and fragmentation efficiencies, even among species with similar structures but different hydrocarbon chain length and/or degrees of unsaturation. This phenomenon was also observed in our study (Fig. 4). Not only did HexCers of different *N*-fatty acyl chain length or degree of unsaturation have very different instrument responses, isomeric GlcCers and GalCers also behaved differently. Therefore, the use of one "class representative" standard (e.g., GlcCer) for the quantification of HexCer will unavoidably skew the quantification. In this study, HexCer subspecies were first separated by RP LC based on retention time, and coeluting isomeric species were further resolved by DMS. The advantage of resolving each subspecies in our method allows the use of subclass-specific isomeric GlcCer(d18:1/8:0) and GalCer(d18:1/8:0) standards for the quantification of GlcCer and GalCer, respectively, and accounts for instrument response differences between subspecies within each subclass with the application of correction factors. In addition, DMS technology also enables sampling in very small quantities of CSF. As human CSF is a scarce and precious resource, particularly from disease-specific biobanks, this method facilitates measurement in the applied neurological research setting.

In summary, DMS technology enables orthogonal selectivity to LC/MS techniques and thus allows for simultaneously quantifying and unambiguously assigning cerebroside lipid species in biological samples. Our results show great promise for the future applications of the DMS technology in the field of GSL analysis for biomarker discovery and drug screening.

The data and biospecimens used in the preparation of this manuscript were obtained from the NINDS PDBP Consortium. Investigators include Roger Albin, Roy Alcalay, Alberto Ascherio, DuBois Bowman, Alice Chen-Plotkin, Ted Dawson, Richard Dewey, Dwight German, Xuemei Huang, Judith Potashkin, Rachel Saunders-Pullman, Liana Rosenthal, Clemens Scherzer, David Vaillancourt, Vladislav Petyuk, David Walt, Andy West, and Jing Zhang. The PDBP investigators other than R. Saunders-Pullman have not participated in reviewing the data analysis or content of this manuscript. The authors thank Avanti Polar Lipids, Inc., for collaborating in custom-synthesizing cerebroside lipid standards and Lisa Connell and Jeff Moore for their critical review of the manuscript. The authors also thank SCIEX for providing the DMS unit on a collaborative research agreement.

## REFERENCES

1. Regina Todeschini, A., and S. I. Hakomori. 2008. Functional role of glycosphingolipids and gangliosides in control of cell adhesion, motility, and growth, through glycosynaptic microdomains. *Biochim. Biophys. Acta.* **1780:** 421–433.
2. Ichikawa, S., H. Sakiyama, G. Suzuki, K. I. Hidari, and Y. Hirabayashi. 1996. Expression cloning of a cDNA for human ceramide glucosyltransferase that catalyzes the first glycosylation step of glycosphingolipid synthesis. *Proc. Natl. Acad. Sci. USA.* **93:** 4638–4643.
3. Schulte, S., and W. Stoffel. 1993. Ceramide UDPgalactosyltransferase from myelinating rat brain: purification, cloning, and expression. *Proc. Natl. Acad. Sci. USA.* **90:** 10265–10269.
4. Kapitonov, D., and R. K. Yu. 1997. Cloning, characterization, and expression of human ceramide galactosyltransferase cDNA. *Biochem. Biophys. Res. Commun.* **232:** 449–453.
5. Bosio, A., E. Binczek, M. M. Le Beau, A. A. Fernald, and W. Stoffel. 1996. The human gene CGT encoding the UDP-galactose ceramide galactosyl transferase (cerebroside synthase): cloning, characterization, and assignment to human chromosome 4, band q26. *Genomics.* **34:** 69–75.
6. Sprong, H., B. Kruithof, R. Leijendekker, J. W. Slot, G. van Meer, and P. van der Sluijs. 1998. UDP-galactose:ceramide galactosyltransferase is a class I integral membrane protein of the endoplasmic reticulum. *J. Biol. Chem.* **273:** 25880–25888.
7. Bosio, A., E. Binczek, and W. Stoffel. 1996. Functional breakdown of the lipid bilayer of the myelin membrane in central and peripheral nervous system by disrupted galactocerebroside synthesis. *Proc. Natl. Acad. Sci. USA.* **93:** 13280–13285.
8. Coetzee, T., N. Fujita, J. Dupree, R. Shi, A. Blight, K. Suzuki, K. Suzuki, and B. Popko. 1996. Myelination in the absence of galactocerebroside and sulfatide: normal structure with abnormal function and regional instability. *Cell.* **86:** 209–219.
9. Yamashita, T., R. Wada, T. Sasaki, C. Deng, U. Bierfreund, K. Sandhoff, and R. L. Proia. 1999. A vital role for glycosphingolipid synthesis during development and differentiation. *Proc. Natl. Acad. Sci. USA.* **96:** 9142–9147.
10. Jennemann, R., R. Sandhoff, L. Langbein, S. Kaden, U. Rothermel, H. Gallala, K. Sandhoff, H. Wiegandt, and H. J. Grone. 2007. Integrity and barrier function of the epidermis critically depend on glucosylceramide synthesis. *J. Biol. Chem.* **282:** 3083–3094.
11. Jennemann, R., R. Sandhoff, S. Wang, E. Kiss, N. Gretz, C. Zuliani, A. Martin-Villalba, R. Jager, H. Schorle, M. Kenzelmann, et al. 2005. Cell-specific deletion of glucosylceramide synthase in brain leads to severe neural defects after birth. *Proc. Natl. Acad. Sci. USA.* **102:** 12459–12464.

12. Schwarz, A., and A. H. Futerman. 1997. Distinct roles for ceramide and glucosylceramide at different stages of neuronal growth. *J. Neurosci.* **17:** 2929–2938.
13. Suzuki, K., and Y. Suzuki. 1970. Globoid cell leucodystrophy (Krabbe's disease): deficiency of galactocerebroside beta-galactosidase. *Proc. Natl. Acad. Sci. USA.* **66:** 302–309.
14. Zhao, H., and G. A. Grabowski. 2002. Gaucher disease: perspectives on a prototype lysosomal disease. *Cell. Mol. Life Sci.* **59:** 694–707.
15. Jmoudiak, M., and A. H. Futerman. 2005. Gaucher disease: pathological mechanisms and modern management. *Br. J. Haematol.* **129:** 178–188.
16. Elstein, D., R. Alcalay, and A. Zimran. 2015. The emergence of Parkinson disease among patients with Gaucher disease. *Best Pract. Res. Clin. Endocrinol. Metab.* **29:** 249–259.
17. Schapira, A. H. 2015. Glucocerebrosidase and Parkinson disease: recent advances. *Mol. Cell. Neurosci.* **66:** 37–42.
18. Li, Y., P. Li, H. Liang, Z. Zhao, M. Hashimoto, and J. Wei. 2015. Gaucher-associated Parkinsonism. *Cell. Mol. Neurobiol.* **35:** 755–761.
19. Beach, D. G., J. E. Melanson, and R. W. Purves. 2015. Analysis of paralytic shellfish toxins using high-field asymmetric waveform ion mobility spectrometry with liquid chromatography-mass spectrometry. *Anal. Bioanal. Chem.* **407:** 2473–2484.
20. Ray, J. A., M. M. Kushnir, R. A. Yost, A. L. Rockwood, and A. Wayne Meikle. 2015. Performance enhancement in the measurement of 5 endogenous steroids by LC-MS/MS combined with differential ion mobility spectrometry. *Clin. Chim. Acta.* **438:** 330–336.
21. Varesio, E., J. C. Y. Le Blanc, and G. Hopfgartner. 2012. Real-time 2D separation by LC × differential ion mobility hyphenated to mass spectrometry. *Anal. Bioanal. Chem.* **402:** 2555–2564.
22. Parson, W. B., B. B. Schneider, V. Kertesz, J. J. Corr, T. R. Covey, and G. J. Van Berkel. 2011. Rapid analysis of isomeric exogenous metabolites by differential mobility spectrometry-mass spectrometry. *Rapid Commun Mass Spectrom.* **25:** 3382–3386.
23. Porta, T., E. Varesio, and G. Hopfgartner. 2013. Gas-phase separation of drugs and metabolites using modifier-assisted differential ion mobility spectrometry hyphenated to liquid extraction surface analysis and mass spectrometry. *Anal. Chem.* **85:** 11771–11779.
24. Li, H., K. Giles, B. Bendiak, K. Kaplan, W. F. Siems, and H. H. Hill, Jr. 2012. Resolving structural isomers of monosaccharide methyl glycosides using drift tube and traveling wave ion mobility mass spectrometry. *Anal. Chem.* **84:** 3231–3239.
25. Kyle, J. E., X. Zhang, K. K. Weitz, M. E. Monroe, Y. M. Ibrahim, R. J. Moore, J. Cha, X. Sun, E. S. Lovelace, J. Wagoner, et al. 2016. Uncovering biologically significant lipid isomers with liquid chromatography, ion mobility spectrometry and mass spectrometry. *Analyst.* **141:** 1649–1659.
26. Baker, P. R., A. M. Armando, J. L. Campbell, O. Quehenberger, and E. A. Dennis. 2014. Three-dimensional enhanced lipidomics analysis combining UPLC, differential ion mobility spectrometry, and mass spectrometric separation strategies. *J. Lipid Res.* **55:** 2432–2442.
27. Lintonen, T. P., P. R. Baker, M. Suoniemi, B. K. Ubhi, K. M. Koistinen, E. Duchoslav, J. L. Campbell, and K. Ekroos. 2014. Differential mobility spectrometry-driven shotgun lipidomics. *Anal. Chem.* **86:** 9662–9669.
28. Bligh, E. G., and W. J. Dyer. 1959. A rapid method of total lipid extraction and purification. *Can. J. Biochem. Physiol.* **37:** 911–917.
29. Granger, M. W., H. Liu, C. F. Fowler, A. P. Blanchard, M. Taylor, S. P. M. Sherman, H. Xu, W. Le, and S. A. L. Bennett. 2018. Distinct disruptions in Land's cycle remodeling of glycerophosphocholines in murine cortex mark symptomatic onset and progression in two Alzheimer's disease mouse models. *J. Neurochem.* Epub ahead of print. July 25 2018; .
30. Schneider, B. B., E. G. Nazarov, F. Londry, P. Vouros, and T. R. Covey. 2016. Differential mobility spectrometry/mass spectrometry history, theory, design optimization, simulations, and applications. *Mass Spectrom. Rev.* **35:** 687–737.
31. Schneider, B. B., T. R. Covey, S. L. Coy, E. V. Krylov, and E. G. Nazarov. 2010. Planar differential mobility spectrometer as a prefilter for atmospheric pressure ionization mass spectrometry. *Int. J. Mass Spectrom.* **298:** 45–54.
32. Eiceman, G. A., E. V. Krylov, N. S. Krylova, E. G. Nazarov, and R. A. Miller. 2004. Separation of ions from explosives in differential mobility spectrometry by vapor-modified drift gas. *Anal. Chem.* **76:** 4937–4944.
33. Schneider, B. B., T. R. Covey, S. L. Coy, E. V. Krylov, and E. G. Nazarov. 2010. Chemical effects in the separation process of a differential mobility/mass spectrometer system. *Anal. Chem.* **82:** 1867–1880.
34. Levin, D. S., P. Vouros, R. A. Miller, E. G. Nazarov, and J. C. Morris. 2006. Characterization of gas-phase molecular interactions on differential mobility ion behavior utilizing an electrospray ionization-differential mobility-mass spectrometer system. *Anal. Chem.* **78:** 96–106.
35. Rorrer Iii, L. C., and R. A. Yost. 2011. Solvent vapor effects on planar high-field asymmetric waveform ion mobility spectrometry. *Int. J. Mass Spectrom.* **300:** 173–181.
36. Tsai, C-W., R. A. Yost, and T. J. Garrett. 2012. High-field asymmetric waveform ion mobility spectrometry with solvent vapor addition: a potential greener bioanalytical technique. *Bioanalysis.* **4:** 1363–1375.
37. Blagojevic, V., G. K. Koyanagi, and D. K. Bohme. 2014. Multicomponent ion modifiers and arcing suppressants to enhance differential mobility spectrometry for separation of peptides and drug molecules. *J. Am. Soc. Mass Spectrom.* **25:** 490–497.
38. Kean, E. L. 1966. Separation of gluco- and galactocerebrosides by means of borate thin-layer chromatography. *J. Lipid Res.* **7:** 449–452.
39. Kaye, E. M., and M. D. Ullman. 1984. Separation and quantitation of perbenzoylated glucocerebroside and galactocerebroside by high-performance liquid chromatography. *Anal. Biochem.* **138:** 380–385.
40. Zama, K., Y. Hayashi, S. Ito, Y. Hirabayashi, T. Inoue, K. Ohno, N. Okino, and M. Ito. 2009. Simultaneous quantification of glucosylceramide and galactosylceramide by normal-phase HPLC using O-phtalaldehyde derivatives prepared with sphingolipid ceramide N-deacylase. *Glycobiology.* **19:** 767–775.
41. Merrill, A. H., Jr., M. C. Sullards, J. C. Allegood, S. Kelly, and E. Wang. 2005. Sphingolipidomics: high-throughput, structure-specific, and quantitative analysis of sphingolipids by liquid chromatography tandem mass spectrometry. *Methods.* **36:** 207–224.
42. Shaner, R. L., J. C. Allegood, H. Park, E. Wang, S. Kelly, C. A. Haynes, M. C. Sullards, and A. H. Merrill, Jr. 2009. Quantitative analysis of sphingolipids for lipidomics using triple quadrupole and quadrupole linear ion trap mass spectrometers. *J. Lipid Res.* **50:** 1692–1707.
43. Ito, M., T. Kurita, and K. Kita. 1995. A novel enzyme that cleaves the N-acyl linkage of ceramides in various glycosphingolipids as well as sphingomyelin to produce their lyso forms. *J. Biol. Chem.* **270:** 24370–24374.
44. Boutin, M., Y. Sun, J. J. Shacka, and C. Auray-Blais. 2016. Tandem mass spectrometry multiplex analysis of glucosylceramide and galactosylceramide isoforms in brain tissues at different stages of Parkinson disease. *Anal. Chem.* **88:** 1856–1863.
45. Nakajima, K., H. Akiyama, K. Tanaka, A. Kohyama-Koganeya, P. Greimel, and Y. Hirabayashi. 2016. Separation and analysis of mono-glucosylated lipids in brain and skin by hydrophilic interaction chromatography based on carbohydrate and lipid moiety. *J. Chromatogr. B Analyt. Technol. Biomed. Life Sci.* **1031:** 146–153.
46. von Gerichten, J., K. Schlosser, D. Lamprecht, I. Morace, M. Eckhardt, D. Wachten, R. Jennemann, H. J. Grone, M. Mack, and R. Sandhoff. 2017. Diastereomer-specific quantification of bioactive hexosylceramides from bacteria and mammals. *J. Lipid Res.* **58:** 1247–1258.
47. Wieland Brown, L. C., C. Penaranda, P. C. Kashyap, B. B. Williams, J. Clardy, M. Kronenberg, J. L. Sonnenburg, L. E. Comstock, J. A. Bluestone, and M. A. Fischbach. 2013. Production of alpha-galactosylceramide by a prominent member of the human gut microbiota. *PLoS Biol.* **11:** e1001610.
48. Kain, L., B. Webb, B. L. Anderson, S. Deng, M. Holt, A. Costanzo, M. Zhao, K. Self, A. Teyton, C. Everett, et al. 2014. The identification of the endogenous ligands of natural killer T cells reveals the presence of mammalian alpha-linked glycosylceramides. *Immunity.* **41:** 543–554. [Erratum. 2014. Immunity. **41:** 867.]
49. Krylov, E. V., S. L. Coy, J. Vandermey, B. B. Schneider, T. R. Covey, and E. G. Nazarov. 2010. Selection and generation of waveforms for differential mobility spectrometry. *Rev. Sci. Instrum.* **81:** 024101.
50. Wells, H. W., and M. Jones. 1973. Galactosylceramides in human plasma. *Am. J. Clin. Pathol.* **60:** 890–896.
51. Vance, D. E., and C. C. Sweeley. 1967. Quantitative determination of the neutral glycosyl ceramides in human blood. *J. Lipid Res.* **8:** 621–630.
52. Quehenberger, O., A. M. Armando, A. H. Brown, S. B. Milne, D. S. Myers, A. H. Merrill, S. Bandyopadhyay, K. N. Jones, S. Kelly, R. L. Shaner, et al. 2010. Lipidomics reveals a remarkable diversity of lipids in human plasma. *J. Lipid Res.* **51:** 3299–3305.
53. Seyer, A., S. Boudah, S. Broudin, C. Junot, and B. Colsch. 2016. Annotation of the human cerebrospinal fluid lipidome using high resolution mass spectrometry and a dedicated data processing workflow. *Metabolomics.* **12:** 91.

**SUPPLEMENTAL INFORMATION:**

# Differential mobility spectrometry as an orthogonal separation to LC-MS/MS for quantification of isomeric cerebrosides in plasma and cerebrospinal fluid

Hongbin Xu[1,2*], Frederic R Boucher[3], Thao T Nguyen[1,2], Graeme P Taylor[1,2], Julianna Tomlinson[4,5], Roberto A Ortega[6], Brigitte Simons[3], Michael Schlossmacher[4,5], Rachel Saunders-Pullman[6,7], Walt Shaw[8], Steffany AL Bennett[1,2,4,5*]

[1]Neural Regeneration Laboratory and India Taylor Lipidomics Research Platform, Ottawa Institute of Systems Biology, Department of Biochemistry, Microbiology, and Immunology, University of Ottawa, Ottawa, Ontario, Canada; [2]Centre for Catalysis Research and Innovation, Department of Chemistry, University of Ottawa, Ottawa, Ontario, Canada; [3]SCIEX, Concord, Ontario, Canada; [4]University of Ottawa Brain and Mind Research Institute, Department of Cellular and Molecular Medicine, University of Ottawa, Ottawa, Ontario, Canada; [5]Neuroscience, Ottawa Hospital Research Institute, Ottawa, Ontario, Canada; [6]Mount Sinai Beth Israel, Neurology, New York, New York, USA; [7]Icahn School of Medicine at Mount Sinai, New York, New York, USA; [8]Avanti Polar Lipids, Inc., Alabaster, Alabama, USA

[*] Co-corresponding authors: hxu@uottawa.ca and sbennet@uottawa.ca

**Supplemental Table S1. Summary of DMS-MS settings**

| **Parameters** | **Settings** |
|---|---|
| Curtain Gas (CUR) | 10 psi |
| Collision Gas (CAD) | 10 psi |
| Ionization Voltage (IS) | 5500 V |
| ESI Source Temperature (TEM) | 250ºC |
| Ion Source Gas1 | 25 psi |
| Ion Source Gas2 | 20 psi |
| Declustering Potential (DP) | 100 V |
| Entrance Potential (EP) | 10 V |
| Collision Energy | Compound dependent |
| Collision Cell Exit Potential (CXP) | 20 V |
| DMS Temperature (DT) | Low, 150ºC |
| DMS Resolution Enhancement (DR) | Medium, 30 psi |
| Modifier Composition (MDC) | Low |
| DMS Separation Voltage (SV) | Compound dependent |
| Compensation Voltage (CoV) | Compound dependent |
| DMS Offset (DMO) | - 3.0 V |
| MRM Transition | $[M + H^+] \longrightarrow 264.3$ |
| Dwell time | 50 ms |

**Supplemental Table S2. MRM transition and optimized SV and CoV values using IPA as the chemical modifier.** Pause between mass ranges was 40 ms.

| ID | Q1 Mass (Da) | Q3 Mass (Da) | Time (ms) | CE (V) | SV (V) | CoV (V) |
|---|---|---|---|---|---|---|
| GlcSph | 462.5 | 264.3 | 20 | 24 | 3100 | -8.8 |
| GalSph | 462.5 | 264.3 | 20 | 24 | 3100 | -7.0 |
| GlcCer(d18:1/8:0) | 588.8 | 264.3 | 20 | 43 | 3200 | -4.6 |
| GalCer(d18:1/8:0) | 588.8 | 264.3 | 20 | 43 | 3200 | -3.3 |
| GlcCer(d18:1/14:0) | 672.5 | 264.3 | 20 | 46 | 3600 | -3.2 |
| GalCer(d18:1/14:0) | 672.5 | 264.3 | 20 | 46 | 3600 | -1.7 |
| GlcCer(d18:1/16:1) | 698.5 | 264.3 | 20 | 49 | 3500 | -2.7 |
| GalCer(d18:1/16:1) | 698.5 | 264.3 | 20 | 49 | 3500 | -1.2 |
| GlcCer(d18:1/16:0) | 700.7 | 264.3 | 20 | 51 | 3600 | -2.5 |
| GalCer(d18:1/16:0) | 700.7 | 264.3 | 20 | 51 | 3600 | -1.0 |
| GlcCer(d18:1/18:1) | 726.6 | 264.3 | 20 | 49 | 3800 | -2.1 |
| GalCer(d18:1/18:1) | 726.6 | 264.3 | 20 | 49 | 3800 | -0.3 |
| GlcCer(d18:1/18:0) | 728.7 | 264.3 | 20 | 51 | 3900 | -1.9 |
| GalCer(d18:1/18:0) | 728.7 | 264.3 | 20 | 51 | 3900 | 0.0 |
| GlcCer(d18:1/20:0) | 756.6 | 264.3 | 20 | 49 | 3600 | -1.2 |
| GalCer(d18:1/20:0) | 756.6 | 264.3 | 20 | 49 | 3600 | 0.3 |
| GlcCer(d18:1/21:0) | 770.7 | 264.3 | 20 | 48 | 3700 | -0.9 |
| GalCer(d18:1/21:0) | 770.7 | 264.3 | 20 | 48 | 3700 | 0.6 |
| GlcCer(d18:1/22:1) | 782.9 | 264.3 | 20 | 47 | 3800 | -1.4 |
| GalCer(d18:1/22:1) | 782.9 | 264.3 | 20 | 47 | 3800 | 0.3 |
| GlcCer(d18:1/22:0) | 784.7 | 264.3 | 20 | 49 | 3700 | -0.9 |
| GalCer(d18:1/22:0) | 784.7 | 264.3 | 20 | 49 | 3700 | 0.7 |
| GlcCer(d18:1/23:0) | 798.7 | 264.3 | 20 | 51 | 3700 | -0.7 |
| GalCer(d18:1/23:0) | 798.7 | 264.3 | 20 | 51 | 3700 | 0.8 |
| GlcCer(d18:1/24:1) | 810.8 | 264.3 | 20 | 51 | 3800 | -0.9 |
| GalCer(d18:1/24:1) | 810.8 | 264.3 | 20 | 51 | 3800 | 0.7 |
| GlcCer(d18:1/24:0) | 812.7 | 264.3 | 20 | 51 | 3600 | -0.8 |
| GalCer(d18:1/24:0) | 812.7 | 264.3 | 20 | 51 | 3600 | 0.7 |
| GlcCer(d18:1/25:0) | 826.9 | 264.3 | 20 | 55 | 3800 | -0.4 |
| GalCer(d18:1/25:0) | 826.9 | 264.3 | 20 | 55 | 3800 | 1.1 |
| GlcCer(d18:1/26:0) | 840.8 | 264.3 | 20 | 55 | 3900 | -0.1 |
| GalCer(d18:1/26:0) | 840.8 | 264.3 | 20 | 55 | 3900 | 1.3 |
| GlcCer(d18:1/31:0) | 911 | 264.3 | 20 | 47 | 4000 | 0.4 |
| GalCer(d18:1/31:0) | 911 | 264.3 | 20 | 47 | 4000 | 1.8 |

**Supplemental Table S3. Precision of the method using human plasma**

| | GlcCer | | | | | | | | | GalCer | | | | |
|---|---|---|---|---|---|---|---|---|---|---|---|---|---|---|
| **FA[#]** | **16:0** | **18:0** | **20:0** | **22:0** | **23:0** | **24:0** | **24:1** | **25:0** | **26:0** | **16:0** | **22:0** | **23:0** | **24:0** | **24:1** |
| **CV%** | 6.1 | 16.5 | 16.5 | 9.8 | 9.1 | 6.3 | 4.5 | 23.2 | 6.7 | 17.4 | 19.9 | 15.6 | 15.0 | 15.4 |

[#] FA denotes carbon number and degree of unsaturation of *N*-fatty acyl chain in the ceramide moiety (e.g., 16:0 for fatty acyl chain with 16 carbons and zero double bonds). CV% was calculated from five sequential runs of the same human plasma lipid extract separated by a blank between runs.

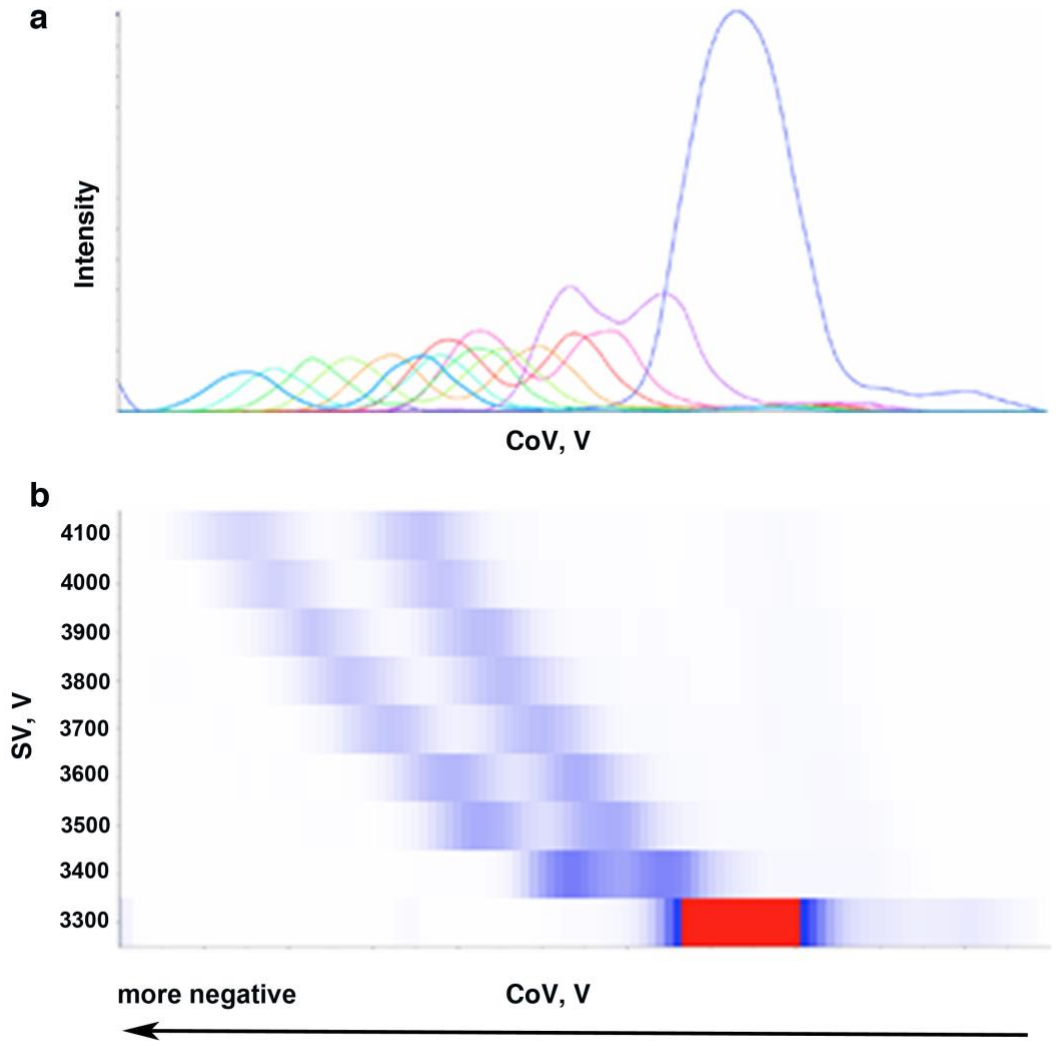


**Supplemental Figure S1. Relationship between separation voltage, detection sensitivity and compensation voltage.** Representative ionograms (a) and corresponding heatmap (b) showing that higher SV shifted the ionograms to the more negative CoV and resulted in better separation but with decreased sensitivity.

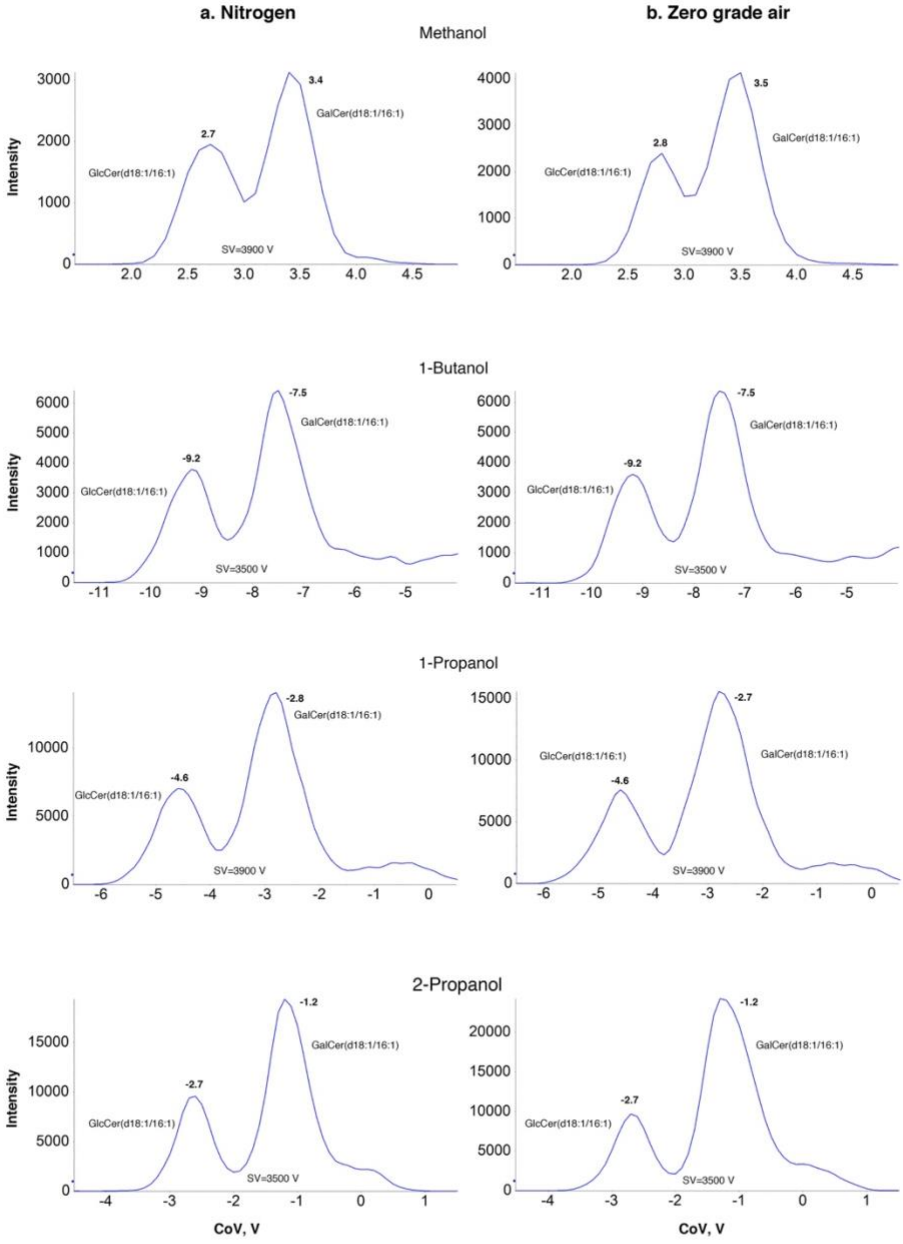
a. Nitrogen
b. Zero grade air
Methanol
1-Butanol
1-Propanol
2-Propanol
Intensity
CoV, V
GlcCer(d18:1/16:1)
GalCer(d18:1/16:1)
SV=3900 V
SV=3500 V
2.7
3.4
2.8
3.5
-9.2
-7.5
-4.6
-2.8
-2.7
-2.7
-1.2
-1.2

**Supplemental Figure S2. Similar DMS performance with either nitrogen or zero grade air as GS1 and GS2.** There was no difference in peak separation, peak shape and signal intensity using either nitrogen (a) or zero grade air (b) as GS1 and GS2 with any of the four chemical modifiers. The optimized CoV values were constant for isomeric standards using either gas.